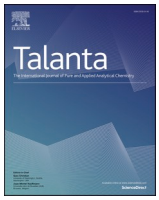
Talanta 280 (2024) 126708



Contents lists available at ScienceDirect

Talanta

journal homepage: www.elsevier.com/locate/talanta





Rapid SARS-CoV-2 sensing through oxygen reduction reaction catalysed by Au@Pt/Au core@shell nanoparticles

Emiliano Martínez-Periñán [a,b], María Palomares-Albarrán [a], Celia Toyos-Rodríguez [c,d], Eva Mateo-Martí [e], Félix Pariente [a,b], Alfredo de la Escosura-Muñiz [c,d], Cristina Gutiérrez-Sánchez [a,b,**], Mónica Revenga-Parra [a,b,*], Encarnación Lorenzo [a,b,f]

[a] Grupo de Sensores Químicos y Biosensores, Departamento de Química Analítica y Análisis Instrumental, Universidad Autónoma de Madrid, 28049, Madrid, Spain
[b] Institute for Advanced Research in Chemical Sciences (IAdChem), Universidad Autónoma de Madrid, 28049, Madrid, Spain
[c] NanoBioAnalysis Group, Departamento de Química Física y Analítica, Universidad de Oviedo, 33006, Oviedo, Spain
[d] Biotechnology Institute of Asturias, Universidad de Oviedo, Edificio Santiago Gascon, 33006, Oviedo, Spain
[e] Centro de Astrobiología (CSIC-INTA), Ctra. Ajalvir, Km. 4, 28850, Torrejón de Ardoz, Madrid, Spain
[f] IMDEA-Nanociencia, Ciudad Universitaria de Cantoblanco, 28049, Madrid, Spain

ARTICLE INFO

Keywords:
COVID-19
SARS-CoV-2
ORF_{1ab} sequence
Bimetallic nanoparticles
Oxygen reduction reaction
DNA biosensor

ABSTRACT

The development of rapid, accurate, sensitive, and low-cost diagnostic methods for COVID-19 detection in real-time is the unique way to control infection sources and monitor illness progression. In this work, we propose an electrochemical biosensor for the rapid and accuracy diagnosis of COVID-19, through the determination of ORF_{1ab} specific sequence. The biosensor is based on the immobilization of a thiolated sequence partially complementary (domain 1) to ORF_{1ab} on gold screen-printed electrodes and the use of bifunctional Au@Pt/Au core@shell nanoparticles modified with a second thiolated sequence partially complementary to ORF_{1ab} (domain 2) as electrochemical indicator of the hybridization of DNA sequences. The synthesized Au@Pt/Au nanoparticles consist of an Au core, a shell of Pt (Au@Pt NPs), that provides an excellent electrocatalytic activity toward the oxygen reduction reaction (ORR) even after formation of hybrid biomaterials by modification, through the Au protuberances growth on the NPs surface, with an oligonucleotide with recognition ability. The ORR electrochemical activity, enhanced by the label element (Au@Pt/Au NPs), has been employed, for the first time, as indicator of the hybridization event. Based on this strategy, target sequences of the SARS-CoV-2 virus have been detected with a detection limit of 32 pM. The selectivity of the biosensor was confirmed by analysing ORF_{1ab} sequence in the presence of DNA sequences from other viruses. The biosensor has been successfully applied to the direct detection of the virus in non-amplified samples of nasopharyngeal swabs from infected and non-infected patients. Results compare well with those obtained through RT-qPCR but our method is more rapid since does not need any amplification process.

1. Introduction

After the pandemic caused by the coronavirus SARS-CoV-2, specially, during autumn and winter, overflow health care workers are struggling as hospitals fill with sick patients battling respiratory illnesses. Different diseases generated by virus (SARS-CoV-2, MERS-CoV, Influenza A, Enterovirus, Rhinovirus and Respiratory Syncytial virus) or bacteria (*Mycobacterium tuberculosis, Mycoplasma pneumoniae, Streptococcus pneumoniae* and *Chlamydophila pneumoniae*) and even more chronic severe respiratory diseases (lung cancer, cystic fibrosis, asthma, or chronic obstructive pulmonary disease, etc.), have similar symptoms [1]. Despite of that, each of them requires specific treatments and

* Corresponding author. Grupo de Sensores Químicos y Biosensores, Departamento de Química Analítica y Análisis Instrumental, Universidad Autónoma de Madrid, 28049, Madrid, Spain.
** Corresponding author. Grupo de Sensores Químicos y Biosensores, Departamento de Química Analítica y Análisis Instrumental, Universidad Autónoma de Madrid, 28049, Madrid, Spain.
E-mail addresses: emiliano.martinez@uam.es (E. Martínez-Periñán), cristina.gutierrezs@uam.es (C. Gutiérrez-Sánchez), monica.revenga@uam.es (M. Revenga-Parra).

https://doi.org/10.1016/j.talanta.2024.126708
Received 21 November 2023; Received in revised form 26 July 2024; Accepted 13 August 2024
Available online 13 August 2024
0039-9140/© 2024 The Author(s). Published by Elsevier B.V. This is an open access article under the CC BY-NC-ND license (http://creativecommons.org/licenses/by-nc-nd/4.0/).

patient's perspectives greatly improve when they are applied as soon as possible. Therefore, an urgent global challenge has emerged, to develop diagnostic technologies that could provide accurate information within a short time frame and so allow to apply an efficient therapy at an early stage [2]. This challenge has been championed by the World Health Organisation (WHO), urging the development of highly sensitive methods capable of operating in robust conditions for the detection of SARS-CoV-2 [3] where biosensors are promising approaches and endorsed by national governments, and highlighted within international consensus. Effective and fast diagnosis of diseases relies on accurate molecular tools that reflect the clinical state of the patient.

Regarding infectious diseases, international and national organizations are involved in the development of sentinel programmes that alert to the spread of infectious diseases [4]. For this purpose, early and accurate detection of the pathogen that is generating the infection is of paramount importance. Current diagnoses of COVID-19 are based mainly on rapid antigen [5] and molecular tests. Although antigen-based approaches present some advantages such as they can be used for mass screening, high specificity, portability and low cost, their greatest drawback is their low sensitivity when compared to molecular tests. On the contrary, molecular tests use reverse transcriptase real-time polymerase chain reaction (RT-PCR), which is a highly sensitive and specific diagnostic. However, these approaches are time consuming, can only be performed in a laboratory and require highly qualified personnel. Hence in this context, point-of-care (POC) devices can provide instantaneous results, supporting the provision of timely patient care by better-informed healthcare professionals [6]. Furthermore, low-trained personnel can easily use these devices and transfer the necessary information.

Among POC devices for infectious pathogen detection, DNA biosensors offer highest sensitivity, accuracy, specificity, selectivity, and simplicity, having been applied for the detection of wide range of viral pathogens in clinical samples [7]. In this context the development of new strategies for DNA biosensor design is a melt pot of analytical chemistry, biochemistry, material science and diagnostic medicine. Among the different kind of DNA biosensors available, optical-based biosensors such as surface plasmon resonance (SPR) [8], surface-enhanced Raman scattering (SERS) [9], or electrical-based DNA biosensors as field effect transistors (FETs) [10], stand out electrochemical-based DNA biosensors that offer rapid, simple, highly sensitive, selective, reliable, and low-cost analytical methods [11].

A key aspect of DNA biosensor development is the DNA/RNA hybridization detection. Different strategies have been described using label-free systems to detect hybridization and DNA quantification. As an example, those based on fluorescence [12], UV–Vis [13] and electrochemical techniques [14] among others. The label-free strategies usually have less complicated designs, less preparation time, reduced cost due to the elimination of complex labels, and scalability. These advantages are severely overwhelmed by the disadvantages such as lack of sensitivity, cross-reactivity, and interference [15].This is the reason why labels such as enzymes, nanoparticles, redox-active molecules, etc. have been employed for biosensor development. The need for ultrasensitive assay of low-abundance RNAs and the trend toward miniaturized devices have made nanomaterials significant, since they can produce a synergic effect between catalytic activity, conductivity, and biocompatibility to accelerate the signal transduction, leading to ultrasensitive detection [11,16–18]. In these terms, the ability to modify nanoparticles with biological recognition elements imparts high selectivity onto devices [19]. Regarding the properties of the metallic nanoparticles that we can use for labelling, we highlight their electrocatalytic activity. Core and shell multilayer bimetallic nanoparticles, made up of different metals, are an important alternative to classical nanoparticles since they present a synergistic effect, combining the properties of different metals. This kind of nanoparticles show enhanced properties because they present surface-enhanced Raman scattering (SERS) [20] and electrocatalytic properties [21–23]. Considering these excellent properties, different basic electrocatalytic reactions have been employed to follow biorecognition event in electrochemical biosensors [24] such as oxygen evolution reaction (OER) [25], oxygen reduction reaction (ORR) [26], H_2O_2 oxidation [27], all of them electrocatalysed by metal nanoparticles. The great electrocatalytic activity of metal nanoparticles have facilitated achievement of the high level of signal amplification needed for the development of ultrasensitive electrochemical affinity biosensors.

In this work an electrochemical DNA biosensor for ORF_{1ab} specific sequence of coronavirus SARS-CoV-2 has been developed using Au@Pt/Au nanoparticles as label agent for ORR electrocatalysis. Unless Au@Pt/Au nanoparticles have been previously used as immunosensor label agents [21,22], it is the first time they are conjugated with an oligonucleotide and employed for the development of DNA biosensors and the first time that their ORR electrocatalytic activity is used to monitor the hybridization event of DNA. The proposed DNA biosensor is based on the immobilization of a thiolated oligonucleotide partially complementary (domain 1) to the ORF_{1ab} target DNA sequence on a disposable gold screen-printed electrode, and the use of a bioconjugate label agent: Au@Pt/Au nanoparticles functionalized with a thiolated oligonucleotide partially complementary to ORF_{1ab} in the domain 2 (see Scheme 1). The proposed DNA biosensor has been successfully applied to the analysis of samples of nasopharyngeal swab from COVID-19 patients, provided by a hospital, without the need of DNA amplification. The ORR electrocatalytic activity of the working electrode increases with the viral load of the patient samples tested.

2. Experimental section

2.1. Chemicals

Sodium Phosphate monobasic monohydrate salt ($NaH_2PO_4{\cdot}H_2O$), Sodium Chloride (NaCl), sulfuric acid (H_2SO_4), 6-Mercapto-1-hexanol (MCH), 1,4-Dithiothreitol (DTT) and DNA oligonucleotides (Table 1) were obtained from Merck (Darmstadt, Germany). Sodium Phosphate dibasic dihydrate salt ($Na_2HPO_4{\cdot}2H_2O$) were obtained from Riedel-deHäen (Seelze, Germany). All the solutions were prepared in ultrapure water, purified with a Millipore Milli-Q-System (18.2 MΩ cm).

2.2. Instrumentation

Electrochemical measurements were carried out using a Autolab PGSTAT302 N potentiostat (Eco-Chemie). Software package GPES 4.9 was used for data acquisition. A screen-printed electrode connector (Metrohm) was used as interface. Electrochemical experiments were performed with Metrohm screen-printed gold electrodes (AuSPE, DRP-C220BT) which integrate a gold working electrode, a silver pseudoreference electrode and a gold auxiliary electrode. All electrochemical studies were performed using a home-made electrochemical cell and a BAS Ag/AgCl/3 M KCl external reference electrode.

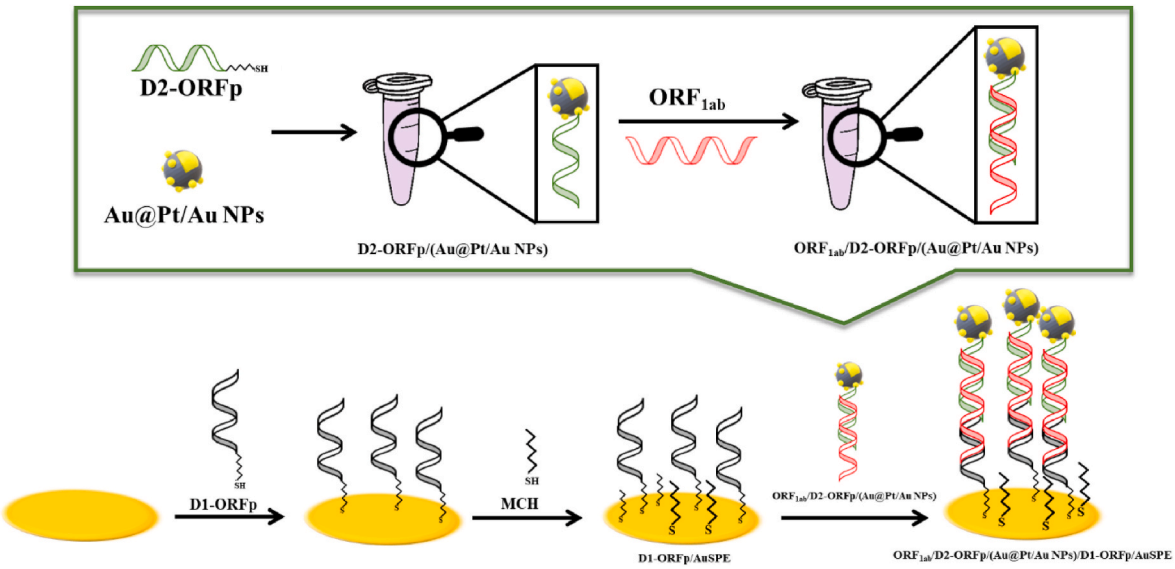
UV–Vis absorption spectra were recorder using a UV-1900 Spectrophotometer from SHIMADZU (Japan) using a low-volume quartz cuvette. UV-Probe software was used for spectra acquisition.

Spectrophotometric measurements of transparent screen-printed gold electrodes (DRP-AUTR10) (Metrohm-DropSens) were carried out using a UV-VIS SPELEC (200–900 nm) in transmission mode.

The high resolution-transmission electron microscopy (HR-TEM) images for were recorder using a FEI Tecnai G2 F20S-TWIN field-emission gun high resolution microscope from FEI (United States of America) on a copper grid, using an accelerating voltage of 200 kV.

Atomic Force Microscopy (AFM) images were taken with an Agilent 5500 microscope and Olympus cantilevers (RC800PSA, 200_20 mm) operating in tapping mode in air on HOPG electrodes.

X-ray Photoelectron Spectroscopy (XPS) analysis of the samples was carried out with a Phoibos 150 MCD spectrometer equipped with hemispherical electron analyzer, and using an Al Ka X-ray source



Scheme 1. Scheme detailing the methodology developed for the design of the biosensor.

Table 1
Oligonucleotide sequences used in this work.

	Sequence	Name
Thiol-Domain 1-probe	5′–SH–C_6H_{10} -CCATAACCTTTCCA-3′	D1-ORFp
Thiol-Domain 2-probe	5′-CATACCGCAGACGG-C_6H_{10} -SH-3′	D2-ORFp
Target	5′-CCGTCTGCGGTATGTGGAAAGGTTATGG-3′	ORF_{1ab}
Interferent 1	5′-CCAGGTGGAAC ATCATCCGGTGATGC-3′	SARS-CoV
Interferent 2	5′ -TTAGTCATCTGCGGGAATGCAGCATTATCT-3′	Influenza A

(1486.7 eV) with an aperture of 7 mm × 20 mm. The base pressure in the ultra-high vacuum chamber was 5×10^{-10} mbar, and the experiments were carried out a room temperature. A 30 eV pass energy was applied for taking the overview sample, whereas 20 eV pass energy was applied for the analysis of the following core level spectra: P (2p) and N (1s). XPS spectra regions were fitted and deconvoluted using the fitt-xps software, calibration was done against the Au (4f 7/2) peak set to 84.0 eV for the NPs gold surface sample.

During the biosensor preparation, a Mini-Shaker PSU-2T from Biosan (Spain) and a thermostatic centrifuge (Universal 320R) from Hettich (Germany) were used.

All material and solutions used in this work were sterilized in a Nüve OT012 autoclave before being used.

2.3. Preparation of SARS-CoV-2 DNA oligonucleotides stock solutions

Prior to use, thiol-modified probe stock solutions (D1-ORFp and D2-ORFp) were prepared following the protocol for thiol-modified oligonucleotide reduction, using a NAP-10 column of Sephadex G-25 (Merck) and 1,4-dithiothreitol (DTT), from Merck. Afterwards, the D1-ORFp probe stock solution was prepared at 10 μM final concentration in 10 mM phosphate buffer (PB) pH 7.0 and the D2-ORFp probe was stored with the initial concentration in 10 mM PB pH 7.0. 100 μM stock solutions of the analyte sequence were prepared using 10 mM PB (pH 7.0) with 0.4 M NaCl as solvent (PBS). All the solutions were stored at −20 °C.

2.4. Bifunctional Au@Pt/Au core@shell nanoparticles synthesis and bioconjugation with D2-ORFp

The synthesis of bimetallic core@shell Au@Pt/Au NPs was carried out following a previously optimized protocol [21]. The procedure starts with the preparation of Turkevich's Au NPs [28], by mixing 80 mL of gold (III) chloride trihydrate (2.94×10^{-4} M) and 2 mL of trisodium citrate (3.88×10^{-2} M), under magnetic stirring for 30 min.

Au NPs were then covered with silver, taking 51.25 mL of the suspension (9.00×10^{14} Au NPs/mL) and mixing it with 3 mL of silver nitrate (5.88×10^{-3} M) and 50 μL of trisodium citrate (3.88×10^{-2} M), boiling for 1h under magnetic stirring. Silver was then replaced by platinum (galvanic replacement) by mixing the obtained suspension with 80 μL of chloroplatinic acid (1.95×10^{-1} M), followed by centrifugation. After re-suspension in water, the obtained core-shell Au@Pt NPs were covered with silver by taking 45 mL of the suspension and mixing it with 1.2 mL of silver nitrate (5.88×10^{-3} M) and 300 μL of trisodium citrate (3.88×10^{-2} M), boiling for 1h under stirring. The last step consists in the formation of Au protuberances replacing the silver, what is performed by mixing the obtained suspension with 150 μL of gold (III) chloride trihydrate (2.94×10^{-4} M) and 150 μL of trisodium citrate (3.88×10^{-2} M), for 20 min under stirring. Finally, the obtained Au@Pt/Au NPs were stored at 4 °C.

The conjugation of the Au@Pt/Au NPs with the detection DNA strand (D2-ORFp) was performed through the well-known thiol-gold affinity. 100 μL of Au@Pt/Au suspension was incubated with D2-ORFp added a volume of PBS to obtain a final concentration of 5.0 μM into an Eppendorf for 30 min at a room temperature in the shaker. After 30 min, the bioconjugate (D2-ORFp/(Au@Pt/Au)) was centrifugated at 12000 rpm, 25 °C for 30 min. The pellet was resuspended in PBS and the solution obtained was sonicated for 15 min.

2.5. SARS-CoV-2 biosensor development

Firstly, AuSPEs were activated in a 0.5 M H_2SO_4 solution by applying ten cyclic scans from −0.2 V to +1.2 V at 0.1 V s^{-1}. Afterwards, AuSPE surfaces were rinsed with water and the working area of the activated AuSPEs was functionalized by thiol chemisorption, coating it with 10 μl of 10 μM D1-ORFp (D1-ORFp/AuSPE) and incubating overnight, at 4 °C. Subsequently, the platforms were rinsed with Milli-Q water to remove unbound materials. Then, 10 μL of blocking solution (1.0 mM MCH) were added to D1-ORFp/AuSPE for 20 min, after that the platforms were

rinsed with Milli-Q water to remove non adsorbed MCH.

Simultaneously, D2-ORFp/(Au@Pt/Au) was hybridized with the analyte, using 10 μL of the standard solution or RNA sample from patients at 40 °C for 1 h using the shaker. After hybridization, ORF_{1ab}/D2-ORFp/(Au@Pt/Au) were incubated with D1-ORFp/AuSPE in humid chamber at 40 °C for 1 h. Finally, the platforms (ORF_{1ab}/D2-ORFp/(Au@Pt/Au NPs)/D1-ORFp/AuSPE) were rinsed with PBS for 30 min, to remove unabsorbed material. Linear sweep voltammetry (LSV) scans were recorded in the range from −0.0 V to −0.7 V at a scan rate of 0.01 V s^{-1} and chronoamperometry (CA) was recorded at a constant potential of −0.55 V for 50 s using a 10 mM pH 7.0 PB O_2-saturated solution electrolyte. −0.55 V were chosen for CA in order to work in the O_2 diffusion regimen of ORR, as the LSV peak was detected at −0.47 V. All electrochemical measurements were recorded in triplicate.

2.6. Detection of RNA SARS-CoV-2 sequences in nasopharyngeal swab samples

With the aim of testing the application of the developed biosensor, nasopharyngeal swab samples obtained from COVID-19 patients' and donated by Hospital La Paz (Madrid) were analysed. Nasopharyngeal swabs were collected in guanidinium thiocyanate-containing viral transport medium (Deltalab, Barcelona, Spain), viral RNA was isolated in a MagMAXTM Express system using the MagMAX CORE Nucleic Acid Purification kit according to the manufacturer instructions. SARS-CoV-2 viral RNA detection and quantification was done using the TaqMan 2019-nCoV Assay Kit v1 (ThermoFisher Scientific). For biosensor application, 10 μL of eluate containing RNA from nasopharyngeal swabs were incubated for 1 h with the bioconjugate D2-ORFp/(Au@Pt/Au) to obtain ORF_{1ab}/D2-ORFp/(Au@Pt/Au) as described in the previous section.

3. Results and discussion

3.1. Synthesis, characterization, and ORR electrocatalytic activity of Au@Pt/Au NPs

Bimetallic Au@Pt/Au NPs made up of Au nucleus coated with Pt, also decorated with small Au incrustations, were prepared following a protocol previously reported by our group [21,22] and others [20]. The chemical route consists of successive metal depositions and galvanic replacement reactions from the starting AuNPs. In the last step of the synthesis, the Au@Pt/Au NPs are obtained from Au@Ag NPs through the action together of both reagent reduction and galvanic replacement, as previously described in detail [29]. Ag structures are first removed by galvanic replacement, so different growth points for Au are formed at the positions where Ag was present. This leads to the formation of Au protuberances rather than a smooth shell. Finally, the later growth of the Au protuberances is attributed to both the Kirkendall effect and the deposition of Au atoms onto the existing Au structures. The size and spherical shape of the Au@Pt/Au NPs was well characterized in the above-mentioned previous works.

It is worthy to note that the starting AuNPs are prepared following the Turkevich's method [28], the gold standard route for the preparation of spherical AuNPs, extensively used for their bioconjugation and application as tags in biosensing. The chemical route for the preparation of the Au@Pt/Au NPs, based on successive metal depositions and galvanic replacement reactions from the starting AuNPs has demonstrated to do not significantly affect neither their roundness nor their bioconjugation ability. In agreement, the NPs prepared in this work are found to be monodispersed, spherical and have an average size of 20 nm as demonstrated by HR-TEM (Fig. 1A). The presence of Au protuberances on the Au@Pt/Au NPs surface was observed (Fig. 1B), also confirming the raspberry-like structure of the Au@Pt/Au NPs. Additionally, elemental composition was determined by EDX spectroscopy, showing the presence of these two elements (Fig. S1).

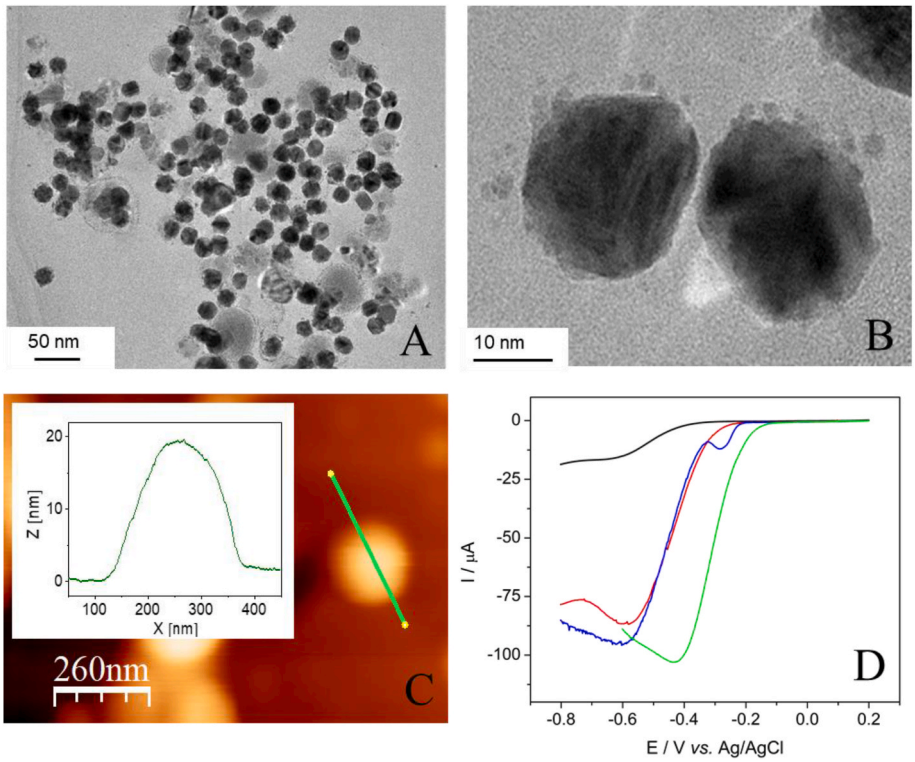


Fig. 1. (A) HR-TEM image of Au@Pt/Au NPs with a magnification of discrete Au@Pt/Au NPs (B). (C) AFM topographic image onto HOPG of Au@Pt/Au NPs, and topographic profile across the green line. (D) LSV at AuSPE (black), Au NPs/AuSPE (red), Pt/Au NPs/AuSPE (blue) and Au@Pt/Au NPs/AuSPE (green) in a O_2-saturated 10 mM PB pH 7.0 solution. Scan rate: 0.01 V s^{-1}.

Moreover, the Au@Pt/Au NPs were characterized by AFM (Fig. 1C), where it is corroborated the spherical shape, and from the profile traced on the nanoparticle a size of 20 nm is estimated. These characterizations demonstrate that the synthesis of Au@Pt/Au NPs has been done successfully in agreement with the above-mentioned previous works.

We proposed the used of Au@Pt/Au NPs as label agent of DNA hybridization event based on their potential ORR electrocatalytic activity, increasing the reduction current and reducing the overpotential associated with the ORR process. For this purpose, the first step was to prove the ORR electrocatalytic activity of Au@Pt/Au NPs. In Fig. 1D it can be observed the LSV obtained in a O_2-saturated 10 mM PB pH 7.0 solution using an unmodified AuSPE (black), and an AuSPEs modified by drop-casting with: Au NPs (red), Pt/Au NPs (blue) and Au@Pt/Au NPs (green). As can be observed, in the case of unmodified AuSPE the ORR onset occurs at −0.45 V *vs.* Ag/AgCl, while the onset potential for the same electrodes modified with Au NPs or Pt/Au NPs starts at −0.30 V *vs.* Ag/AgCl. Furthermore, the cathodic current intensity is clearly the lowest compared with the used of the other metal nanoparticles assayed in this work. Unless the presence of Pt in the NPs' nanostructures does not enhance in a great manner the onset potential of the Au NPs modified electrodes, the current intensity increased, which one would expect that result on a greater sensitivity of the final biosensor. This enhancement is more pronounced when Au@Pt/Au NPs are employed instead of simple bimetallic (Pt/Au) nanoparticles. Furthermore, the onset potential is reduced at −0.15 *vs.* Ag/AgCl, which is an advantage in terms of better sensitivity and avoiding huge overpotential that can lead into interferences. This experiment clearly showed the double benefit of using Au@Pt/Au NPs by one hand as efficient ORR electrocatalyst and at the same time allowing modification with thiolated DNA sequences thanks to the Au atoms surrounding the Pt/Au nanoparticle.

3.2. Characterization of D2-ORFp/(Au@Pt/Au) bioconjugate

The presence of gold protuberances in the Au@Pt/Au NP surface makes it possible to conjugate them with biomolecules to form nanohybrids. In this work, the formation of bioconjugates between Au@Pt/Au NP and thiolated DNA probes was carried out thanks to the well-known thiol-gold affinity. Both components were mixed and allowed to react, as described in the experimental section. The bioconjugate formed D2-ORFp-Au@Pt/Au NPs was characterized by UV–Vis absorbance spectroscopy. We studied the changes produced in the variation of the UV–Vis spectra of Au@Pt/Au and D2-ORFp-Au@Pt/Au NPs (Fig. 2A). Au@Pt/Au NPs UV–Vis spectrum only showed a band centred at 560 nm (black) associated with the plasmon resonance absorption. A slight wavelength shift was observed up to 530 nm when Au@Pt/Au NPs were modified with D2-ORFp sequence. This shift, assigned to changes in the NPs surface plasmon resonance, indicates an interaction between Au@Pt/Au NPs and D2-ORFp [21,22]. In addition, a decrease in absorption is also observed which is consistent with a shielding of the plasmon band of the nanoparticles when they are covered with the DNA sequence. Finally, a band at 254 nm associated with DNA presence can also be observed.

In order to deepen in the bioconjugate formation, we present a characterization of the spectroscopic XPS features for the Au@Pt/Au NPs before and after the D2-ORFp immobilization on the NPs surface. The detection of the P (2p) signal at 133.5 eV associated to the phosphate groups of the DNA backbone and the N (1s) signal after DNA immobilization are an unambiguous signature of the successful modification of the Au@Pt/Au NPs surface with the DNA probe (Figs. S2A–B). The N (1s) XPS core level peak of DNA structure is decomposed in curves components, and every component assigned to different chemical species (Fig. S2C). We can assign the component at the lowest binding

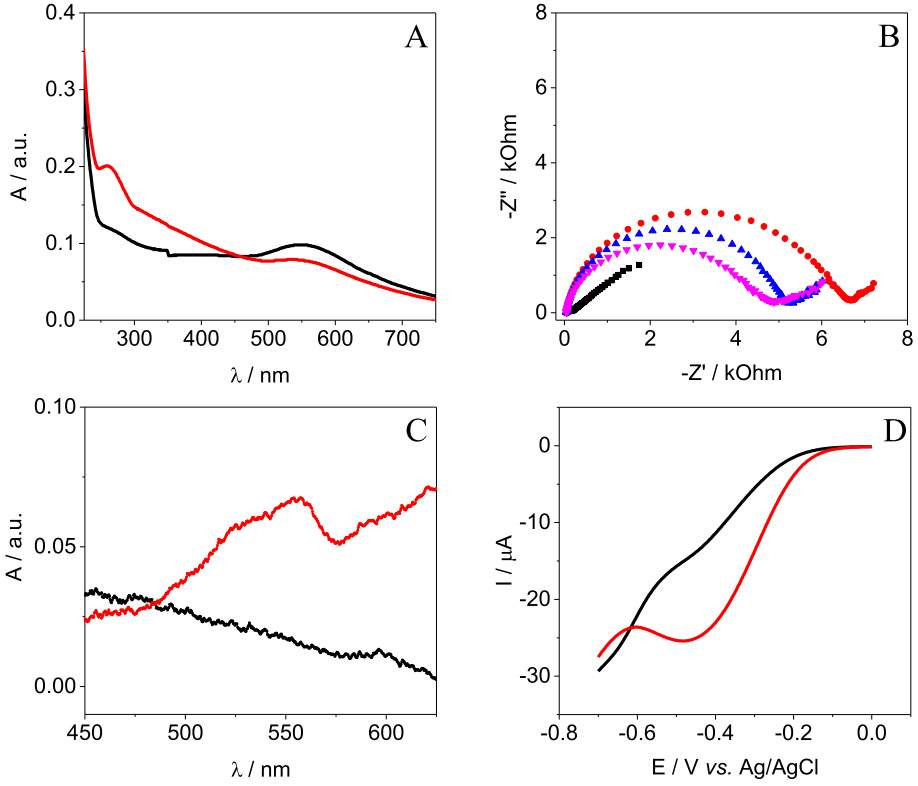


Fig. 2. (A) UV–Vis absorption spectra of Au@Pt/Au NPs (black) and D2-ORFp-Au@Pt/Au NPs (red) in aqueous solution. (B) Nyquist plot recorded in 0.1 M PB, pH 8.0 with 25 mM KCl and 10 mM $K_3Fe(CN)_6$/10 mM $K_4Fe(CN)_6$ at a AuSPE (■), D1-ORFp/AuSPE (●), ORF_{1ab}/D2-ORFp/(Au@Pt/Au NPs)/D1-ORFp/AuSPE (▼) and ORF_{1ab}/D2-ORFp/D1-ORFp/AuSPE (▲). (C) Visible absorption spectra from D1-ORFp/tAuSPE (black) and ORF_{1ab}/D2-ORFp/(Au@Pt/Au NPs)/D1-ORFp/tAuSPE (red) taking as reference the spectrum of tAuSPE. (D) LSV in O_2-saturated 10 mM PB pH 7.0 at D1-ORFp/AuSPE after incubation with the bioconjugates (D2-ORFp/(Au@Pt/Au NPs)) (black) and (ORF_{1ab}/D2-ORFp/(Au@Pt/Au NPs)) (red). Scan rate: 0.01 V s^{-1}.

energy, 398.7 eV, to the nitrogen with unsaturated chemical bonds (-N =). The second peak, at 399.8 eV to the nitrogen (–NH–) from two different contributions: amide group and nucleic bases rings plus a contribution of N with three single bonds. All these forms of N present similar binding energies and therefore in our spectra are within a single wide peak at 399.8 eV. Finally, the peak at 401.1 eV of binding energy agrees well with $–NH_2$ nitrogen from nucleic bases rings [30] corroborating the appearance of the characteristics DNA fingerprints on the D2-ORFp-Au@Pt/Au NPs bioconjugate.

3.3. Characterization of the proposed SARS-CoV-2 biosensor

In this work we present a sensitive and selective methodology to detect SARS-CoV-2 sequences based on the use of a bioconjugate formed by bifunctional Au@Pt/Au core@shell nanoparticles modified with a thiolated sequence partially complementary to the target DNA, as an electrochemical indicator of the hybridization of DNA sequences. As is depicted in Scheme 1, after hybridization of the bioconjugate formed by the Au@Pt/Au NPs with the D2-ORFp detection DNA strand (D2-ORFp/(Au@Pt/Au NPs) with the target (ORF_{1ab}), the resulting double stranded bioconjugate (ORF_{1ab}/D2-ORFp/(Au@Pt/Au NPs) was added to the biosensing platform, consisting in a gold electrode modified with the corresponding thiolated capture probe. Recognition of the target, present in the double-stranded bioconjugate (ORF_{1ab}/D2-ORFp/(Au@Pt/Au NPs), by the capture probe on the surface of the biosensing platform results in a modified electrode carrying the Au@Pt/Au NPs, which are used as electrochemical indicators of the hybridization evet. The detection and quantification of DNA target molecule, which contains a region of the SARS-CoV-2 sequence, is carried out using an O_2-saturated electrolyte by the ORR electrocatalytic activity of the Au@Pt/Au NPs. The difference between the signal response in the absence and in the presence of the target DNA allows the presence of the target DNA in the sample to be detected.

Since electrochemical impedance analysis (EIS) is a powerful tool for studying the interfacial properties of modified electrodes, we use this technique to monitor changes in the properties of the electrode surface in the different steps during biosensor fabrication. Nyquist diagrams obtained using a 0.1 M PB, pH 8.0 solution with 25 mM KCl and 10 mM $K_3Fe(CN)_6$/10 mM $K_4Fe(CN)_6$ are showed at Fig. 2B. At first, the bare AuSPE showed a charge transfer resistance (R_{CT}) value of 0.2 kΩ. When the thiolated DNA probe (D1-ORFp) was chemisorbed on the AuSPE, a huge increase of R_{CT} was observed, increasing until 6.6 kΩ. This result evinces that the DNA probe has been chemisorbed over the gold working electrode, increasing the charge transfer resistance of the redox probe. After that, the electrochemical platform was incubated with the bioconjugate labelling agent D2-ORFp/(Au@Pt/Au), after being incubated with the target DNA sequence, (ORF_{1ab}/D2-ORFp/(Au@Pt/Au NPs)). As can be seen, the R_{CT} decreases until 4.7 kΩ, associated with two phenomena: the increase of the electron transfer rate due to the presence of Au@Pt/Au, and because of the DNA hybridization, which increases the DNA stranded stiffness, allowing an increase of the redox probe permeability through the monolayer. To confirm this second statement, an experiment incubating D1-ORFp/AuSPE with ORF_{1ab}/D2-ORFp was also carried out, showing a decrease in R_{CT} value (5.2 kΩ) compared with D1-ORFp/AuSPE obtained data. All these experiments allow us to confirm the correct modification of the AuSPE electrode surface during all the steps in the development of the biosensor proposed.

To deepen the electrochemical platform characterization, we have also employed visible absorbance spectroscopy employing gold transparent screen-printed electrodes modified in the same way as conventional electrodes (Fig. 2C). The spectrum of the optically transparent AuSPE modified with the chemisorbed DNA probe (D1-ORFp/tAuSPE) does not show significant differences compared to the reference spectrum (using just a non-modified optically transparent AuSPE), since no new bands are observed (black spectrum). However, when the D2-ORFp/(Au@Pt/Au) bioconjugate is hybridized with D1-ORFp/tAuSPE, the spectrum (red spectrum) shows the characteristic band at 560 nm attributed to the presence of Au@Pt/Au (section 3.2). These results clearly show that after the hybridization step, the Au@Pt/Au NPs are retained on the working electrode surface and are the responsible for the enhancement in ORR electrocatalytic activity, as will be demonstrated below.

Once we proved by different techniques the hybridization of D1-ORFp/AuSPE with the double stranded bioconjugate ORF_{1ab}/D2-ORFp/(Au@Pt/Au NPs), showing that the biorecognition event had taken place, the next step was to characterize the electrochemical response of the biosensing platform. For this purpose, we followed the ORR electrocatalytic activity using voltammetric techniques, in particular, LSV. The ORR electrocatalytic response of the platform D1-ORFp/AuSPE was recorded after the incubation of the platform D1-ORFp/AuSPE with both bioconjugates, the ones resulting before (D2-ORFp/(Au@Pt/Au NPs)) and after (ORF_{1ab}/D2-ORFp/(Au@Pt/Au NPs)) hybridization with the target DNA (1.0 nM ORF_{1ab}) (Fig. 2D). As one would expect, when the target DNA is present in the sample the ORR electrocatalytic current increases due to the electrocatalytic activity of the Au@Pt/Au NPs, now present on the biosensing platform because the hybridization between the probe (D1-ORFp) and the bioconjugate (see Scheme 1), towards the ORR. In addition, it can be observed that the oxygen reduction process occurs at a lower potential, due to the electrocatalytic activity of Au@Pt/Au NPs. This result confirms the success of the biosensor development, showing a clear difference between the signal response in the absence and in the presence of the target DNA.

At this point, different aspects of the biosensor development were optimized. This information is included in SI1 and Fig. S3 in the Supporting Information.

The analytical properties of the biosensor were studied under the optimal experimental conditions selected above. The chronoamperometric responses were recorded at −0.55 V *vs.* Ag/AgCl in O_2-saturated 10 mM PB pH 7.0 solution (Fig. 3A). This potential value is around 80 mV after the ORR peak potential (−0.47 V) in order to ensure that we are measuring the maximum steady state current, and to work in the O_2 diffusion regimen of ORR. The current increases as the ORF_{1ab} concentration increases. Fig. 3B shows how the cathodic current response (at 50 s) is proportional to the log [ORF_{1ab}] in the concentration range under study (5.0×10^{-2} – 5.0 nM), fitting to the equation: I(μA)= (−5.6 ± 0.2) log([ORF_{1ab}]/(nM)) – (27.6 ± 0.2), R^2 = 0.993. The limit of detection (LD) was calculated as the blank signal minus three times the standard deviation of the blank signal divided by the slope of the semilogarithmic curve. The value obtained has been expressed in concentration units and was found to be 32 pM.

An important aspect to consider for the analytical application of a biosensor is its selectivity. That is its response to potential interferents. Hence, the selectivity of the biosensor developed was evaluated by measuring its response after the incubation of the bioconjugate with the SARS-CoV-2 target sequence ([ORF_{1ab}] = 1.0 nM) in the presence of another viruses DNA sequences like SARS-CoV and Influenza A, at the same concentration (1.0 nM) of the target sequence. As can be seen in Fig. 3C, the biosensor response is not affected by the presence of other potentially interfering virus sequences.

The stability of both D1-ORFp/AuSPE platform and D2-ORFp/(Au@Pt/Au NPs) bioconjugate were also evaluated. In the first case, the modified electrodes were stored at 4 °C for several weeks. The biosensor can detect the ORF_{1ab} target sequence over a period of six weeks. Furthermore, the ability of the bioconjugate to recognize the target sequence was evaluated over time, obtaining similar current signals for 4 weeks. At this time, no aggregation was observed in the bioconjugate solution.

The biosensor properties have been compared with other previously reported in different articles (Table S1). Unless some articles reported really amazing limits of detection in the recognition of ORF_{1ab} sequence, our work still present good analytical parameters as sensibility, limit of detection, reproducibility and furthermore is based on a simple and

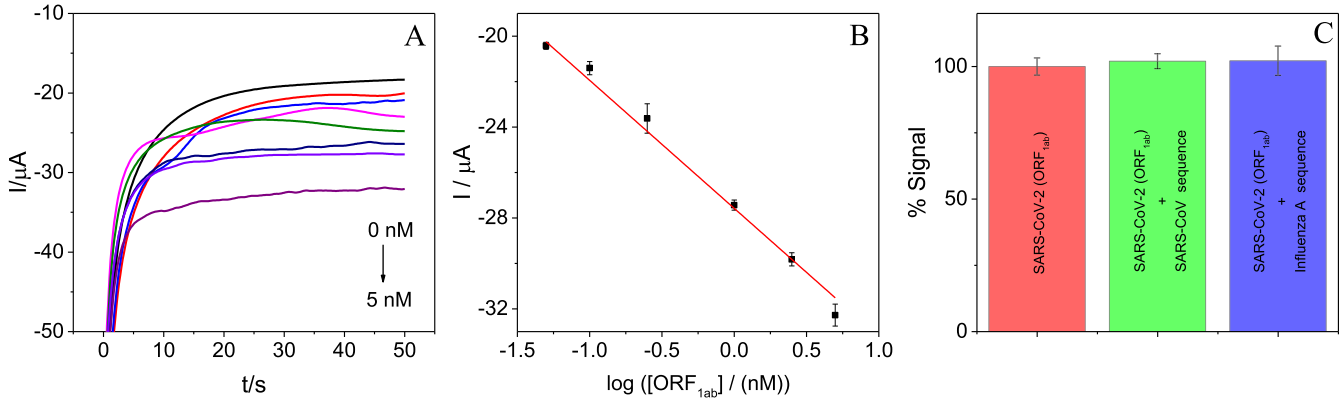


Fig. 3. (A) Chronoamperograms recorded applying −0.55 V *vs.* Ag/AgCl in O_2-saturated 10 mM PB pH 7.0 for different ORF_{1ab} concentrations. (B) Calibration plot obtained from the chronoamperometric data of A. The error bars correspond to the standard deviation obtained by measuring the response of six different biosensors (n = 6). (C) Biosensor responses to 1.0 nM ORF_{1ab} obtained in the absence and in presence of 1.0 nM different potential interfering sequences (n = 3).

selective methodology with short analysis time and without the need of any amplification process. All these good properties aim us to use our developed biosensor in the direct analysis of nasopharyngeal swab samples from COVID-19 patients.

3.4. Analysis of SARS-CoV-2 in nasopharyngeal swab samples

Detection of SARS-CoV-2 in clinical nasopharyngeal swab samples from CoV-2 patients, provided by Hospital La Paz (Spain), was carried out using the developed biosensor with excellent results and avoiding any amplification process. For the sample analyses, 10 μL of nasopharyngeal swab were incubated for 1 h with the bioconjugate and after hybridization the complete bioconjugate was incubated for 1 h on the biosensing surface. For positive and negative diagnosis, the different chronoamperometric responses were evaluated. A clear difference between a negative COVID-19 samples (non-infected patient) used as control and multiple (10) positive COVID-19 patient samples has been observed (Fig. 4). The negative sample gives a response barely the same as the blank. However, positive samples with different viral load give high biosensor responses (indicated as % increment respect to the blank), clearly distinguishable from the negative one. We want also to remark that in the analysis of these samples we have directly measured RNA from the virus (SARS-CoV-2) without any amplification step, being applied the sample directly after RNA extraction.

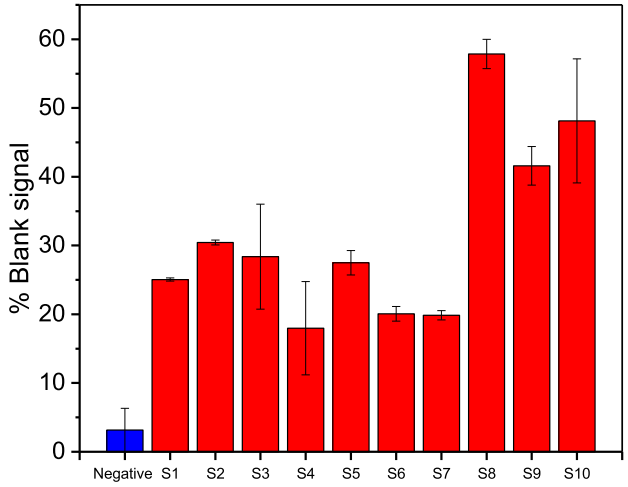


Fig. 4. Blank signal increment percentage using the developed biosensor of a negative COVID-19 patient sample and positive COVID-19 patient samples.

4. Conclusions

A bioconjugate formed by Au@Pt/Au core@shell nanoparticles modified with a thiolated sequence partially complementary to the target DNA has been employed for the first time as electrochemical indicator of the hybridization of DNA sequences, through ORR. The synthesized Au@Pt/Au core@shell nanoparticles, consisting of an Au core and a shell of Pt (Au@Pt NPs), has a double function since they provide an excellent electrocatalytic activity toward the through the ORR, and the Au protuberances growth on their surface allow bioconjugation with a thiolated oligonucleotide as label. Based on this detection system of DNA hybridization, a new biosensor for the rapid and sensitive detection of RNA sequences of SARS-CoV-2, without the need of any amplification process, has been developed. The ORR current catalysed by bifunctional Au@Pt/Au core@shell nanoparticles gives the biosensor signal response. The biosensor shows a semilogarithmic relationship between the current intensity and the concentration of the target and no crossing reactivity. It has been applied to detect the virus in nasopharyngeal swab samples from patients. The results demonstrate that the developed methodology can clearly discriminate between non-infected and infected patient samples. The system has a high sensitivity and a broad applicability since it can be applied to detect any other DNA/RNA sequences related to other pathogens.

CRediT authorship contribution statement

Emiliano Martínez-Periñán: Writing – original draft, Investigation, Formal analysis. **María Palomares-Albarrán:** Investigation. **Celia Toyos-Rodríguez:** Investigation. **Eva Mateo-Martí:** Writing – review & editing, Formal analysis. **Félix Pariente:** Funding acquisition, Conceptualization. **Alfredo de la Escosura-Muñiz:** Writing – original draft, Supervision, Funding acquisition. **Cristina Gutiérrez-Sánchez:** Writing – original draft, Supervision, Funding acquisition, Conceptualization. **Mónica Revenga-Parra:** Writing – original draft, Supervision, Funding acquisition, Conceptualization. **Encarnación Lorenzo:** Writing – original draft, Supervision, Funding acquisition, Conceptualization.

Declaration of competing interest

None.

Data availability

Data will be made available on request.

Acknowledgments

The authors wish to express their sincere thanks to the Spanish Ministerio de Ciencia e Innovación (MICINN) (PID2020-116728RB-I00, PID2020-115204RB-I00, PID2022-140180OB-C22, PID2022-142262OA-I00, TED2021-129738B–I00, RED2022-134120-T) and the Comunidad Autónoma de Madrid (S2018/NMT-4349 TRANS-NANOAVANSENS-CM Program, SI3/PJI/2021–00341) for the financial support. The authors also acknowledge the Microbiology Service and the Biobank of the La Paz University Hospital for preparing and providing COVID-19 samples and Santos Gálvez-Martínez for his collaboration in XPS measurements.

Appendix A. Supplementary data

Supplementary data to this article can be found online at https://doi.org/10.1016/j.talanta.2024.126708.

References

[1] D.F.M. Reukers, L. van Asten, P.S. Brandsema, F. Dijkstra, J.M.T. Hendriksen, M. Hooiveld, F. Jongenotter, M.M.A. de Lange, A.C. Teirlinck, G. Willekens, A. Meijer, A.B. van Gageldonk-Lafeber, Annual report Surveillance of COVID-19, influenza and other respiratory infections in The Netherlands: winter 2021/2022. http://hdl.handle.net/10029/626085, 2022.

[2] V. Subbiah, The next generation of evidence-based medicine, Nat Med 29 (2023) 49–58, https://doi.org/10.1038/s41591-022-02160-z.

[3] A.S. Fauci, H.C. Lane, R.R. Redfield, Covid-19 — navigating the uncharted, N. Engl. J. Med. 382 (2020) 1268–1269, https://doi.org/10.1056/NEJMe2002387.

[4] M.P. Grobusch, L. Weld, J.L. Schnyder, C.S. Larsen, A.K. Lindner, C.P. Popescu, R. Huits, A. Goorhuis, P. Gautret, P. Schlagenhauf, COVID-19 impact on EuroTravNet infectious diseases sentinel surveillance in Europe, Travel Med Infect Dis 53 (2023) 102583, https://doi.org/10.1016/j.tmaid.2023.102583.

[5] S. Suleman, S.K. Shukla, N. Malhotra, S.D. Bukkitgar, N.P. Shetti, R. Pilloton, J. Narang, Y. Nee Tan, T.M. Aminabhavi, Point of care detection of COVID-19: advancement in biosensing and diagnostic methods, Chem. Eng. J. 414 (2021) 128759, https://doi.org/10.1016/j.cej.2021.128759.

[6] N.P. Pai, C. Vadnais, C. Denkinger, N. Engel, M. Pai, Point-of-Care testing for infectious diseases: diversity, complexity, and barriers in low- and middle-income countries, PLoS Med. 9 (2012) e1001306, https://doi.org/10.1371/journal.pmed.1001306.

[7] A. Babaei, A. Pouremamali, N. Rafiee, H. Sohrabi, A. Mokhtarzadeh, M. de la Guardia, Genosensors as an alternative diagnostic sensing approaches for specific detection of virus species: a review of common techniques and outcomes, TrAC, Trends Anal. Chem. 155 (2022) 116686, https://doi.org/10.1016/j.trac.2022.116686.

[8] S.A. Taya, M.G. Daher, A.H.M. Almawgani, A.T. Hindi, S.H. Zyoud, I. Colak, Detection of virus SARS-CoV-2 using a surface plasmon resonance device based on BiFeO3-graphene layers, Plasmonics 18 (2023) 1441–1448, https://doi.org/10.1007/s11468-023-01867-0.

[9] E. Pyrak, J. Krajczewski, A. Kowalik, A. Kudelski, A. Jaworska, Surface enhanced Raman spectroscopy for DNA biosensors—how far are we? Molecules 24 (2019) https://doi.org/10.3390/molecules24244423.

[10] Y. Zhang, B. Chen, D. Chen, Y. Wang, Q. Lu, J. Tan, L. Chen, L. Zhou, W. Tan, Y. Yang, Q. Yuan, Electrical detection assay based on programmable nucleic acid probe for efficient single-nucleotide polymorphism identification, ACS Sens. 8 (2023) 2096–2104, https://doi.org/10.1021/acssensors.3c00453.

[11] S. Campuzano, M. Pedrero, J.M. Pingarrón, Electrochemical genosensors for the detection of cancer-related miRNAs, Anal. Bioanal. Chem. 406 (2014) 27–33, https://doi.org/10.1007/s00216-013-7459-z.

[12] W. Wang, T. Kong, D. Zhang, J. Zhang, G. Cheng, Label-free MicroRNA detection based on fluorescence quenching of gold nanoparticles with a competitive hybridization, Anal. Chem. 87 (2015) 10822–10829, https://doi.org/10.1021/acs.analchem.5b01930.

[13] W. Shen, H. Deng, Y. Ren, Z. Gao, A real-time colorimetric assay for label-free detection of microRNAs down to sub-femtomolar levels, Chem. Commun. 49 (2013) 4959–4961, https://doi.org/10.1039/C3CC41565A.

[14] T. García, E. Casero, M. Revenga-Parra, F. Pariente, E. Lorenzo, Dual-stage DNA sensing: recognition and detection, Anal. Chem. 80 (2008) 9443–9449, https://doi.org/10.1021/ac801558b.

[15] A. Koyappayil, M.-H. Lee, Ultrasensitive materials for electrochemical biosensor labels, Sensors 21 (2021), https://doi.org/10.3390/s21010089.

[16] H. Šípová, S. Zhang, A.M. Dudley, D. Galas, K. Wang, J. Homola, Surface plasmon resonance biosensor for rapid label-free detection of microribonucleic acid at subfemtomole level, Anal. Chem. 82 (2010) 10110–10115, https://doi.org/10.1021/ac102131s.

[17] E.A. Lusi, M. Passamano, P. Guarascio, A. Scarpa, L. Schiavo, Innovative electrochemical approach for an early detection of microRNAs, Anal. Chem. 81 (2009) 2819–2822, https://doi.org/10.1021/ac8026788.

[18] S.-Y. Hou, Y.-L. Hsiao, M.-S. Lin, C.-C. Yen, C.-S. Chang, MicroRNA detection using lateral flow nucleic acid strips with gold nanoparticles, Talanta 99 (2012) 375–379, https://doi.org/10.1016/j.talanta.2012.05.067.

[19] J. Wang, Nanomaterial-based electrochemical biosensors, Analyst 130 (2005) 421–426, https://doi.org/10.1039/B414248A.

[20] W. Xie, C. Herrmann, K. Kömpe, M. Haase, S. Schlücker, Synthesis of bifunctional Au/Pt/Au core/shell nanoraspberries for in situ SERS monitoring of platinum-catalyzed reactions, J. Am. Chem. Soc. 133 (2011) 19302–19305, https://doi.org/10.1021/ja208298q.

[21] A. Iglesias-Mayor, O. Amor-Gutiérrez, A. Novelli, M.-T. Fernández-Sánchez, A. Costa-García, A. de la Escosura-Muñiz, Bifunctional Au@Pt/Au core@shell nanoparticles as novel electrocatalytic tags in immunosensing: application for Alzheimer's disease biomarker detection, Anal. Chem. 92 (2020) 7209–7217, https://doi.org/10.1021/acs.analchem.0c00760.

[22] A.M. Villa-Manso, T. Guerrero-Esteban, F. Pariente, C. Toyos-Rodríguez, A. de la Escosura-Muñiz, M. Revenga-Parra, C. Gutiérrez-Sánchez, E. Lorenzo, Bifunctional Au@Pt/Au nanoparticles as electrochemiluminescence signaling probes for SARS-CoV-2 detection, Talanta 260 (2023) 124614, https://doi.org/10.1016/j.talanta.2023.124614.

[23] X.-R. Li, M.-C. Xu, H.-Y. Chen, J.-J. Xu, Bimetallic Au@Pt@Au core–shell nanoparticles on graphene oxide nanosheets for high-performance H2O2 bi-directional sensing, J. Mater. Chem. B 3 (2015) 4355–4362, https://doi.org/10.1039/C5TB00312A.

[24] L. Ding, A.M. Bond, J. Zhai, J. Zhang, Utilization of nanoparticle labels for signal amplification in ultrasensitive electrochemical affinity biosensors: a review, Anal. Chim. Acta 797 (2013) 1–12, https://doi.org/10.1016/j.aca.2013.07.035.

[25] X. Wei, X. Qiao, J. Fan, H. Dong, Y. Zhang, Y. Zhou, M. Xu, Electrochemiluminescence biosensor for carcinoembryonic antigen detection based on Au-Ag/g-C3N4 nanocomposites, Arab. J. Chem. 15 (2022) 104092, https://doi.org/10.1016/j.arabjc.2022.104092.

[26] C. Leng, J. Wu, Q. Xu, G. Lai, H. Ju, F. Yan, A highly sensitive disposable immunosensor through direct electro-reduction of oxygen catalyzed by palladium nanoparticle decorated carbon nanotube label, Biosens. Bioelectron. 27 (2011) 71–76, https://doi.org/10.1016/j.bios.2011.06.017.

[27] Y. Fu, P. Li, T. Wang, L. Bu, Q. Xie, X. Xu, L. Lei, C. Zou, J. Chen, S. Yao, Novel polymeric bionanocomposites with catalytic Pt nanoparticles label immobilized for high performance amperometric immunoassay, Biosens. Bioelectron. 25 (2010) 1699–1704, https://doi.org/10.1016/j.bios.2009.12.010.

[28] J. Turkevich, P.C. Stevenson, J. Hillier, A study of the nucleation and growth processes in the synthesis of colloidal gold, Discuss. Faraday Soc. 11 (1951) 55–75, https://doi.org/10.1039/DF9511100055.

[29] W. Xie, C. Herrmann, K. Kömpe, M. Haase, S. Schlücker, Synthesis of bifunctional Au/Pt/Au core/shell nanoraspberries for in situ SERS monitoring of platinum-catalyzed reactions, J. Am. Chem. Soc. 133 (2011) 19302–19305, https://doi.org/10.1021/ja208298q.

[30] E. Mateo-Martí, C. Briones, C.M. Pradier, J.A. Martín-Gago, A DNA biosensor based on peptide nucleic acids on gold surfaces, Biosens. Bioelectron. 22 (2007) 1926–1932, https://doi.org/10.1016/j.bios.2006.08.012.